Microscopic description of excitation of nuclear isoscalar giant resonances by inelastic scattering of 240 MeV α particles

A. Kolomiets, O. Pochivalov, and S. Shlomo
Cyclotron Institute, Texas A&M University, College Station, Texas 77843
(Received 22 June 1999; published 17 February 2000)

A microscopic description of the excitation of isoscalar giant monopole resonance (ISGMR) and quadrupole resonance (ISGQR) in ^{28}Si, ^{40}Ca, ^{58}Ni, and ^{116}Sn by 240 MeV bombarding energy α particles is provided based on self-consistent Hartree-Fock– (HF-) random-phase-approximation (RPA) approach and the distorted-wave Born approximation (DWBA). The folding model is used to obtain optical potentials from the HF ground-state density and a density dependent Gaussian nucleon-α interaction ($V_{\alpha n}$). The parameters of $V_{\alpha n}$ are determined by fitting experimentally measured angular distributions for the case of elastic scattering. Angular distributions of inelastically scattered α particles for ISGMR and ISGQR excitations of the target nucleus are obtained using the folding model DWBA and both microscopic (RPA) and hydrodynamical (collective model) transition densities (found from HF ground state densities). A possible overestimation of the energy weighted sum rules and shifts of centroid energies due to the collective-model-based DWBA reaction description is reported.

PACS number(s): 24.30.Cz, 21.60.Jz, 25.55.Ci

I. INTRODUCTION

The study of nuclear giant resonances has long been a subject of extensive theoretical and experimental research [1]. Among the most extensively studied isoscalar resonances are isoscalar giant monopole resonance (ISGMR) and isoscalar giant quadrupole resonance (ISGQR). The determination of parameters describing ISGMR excitation in both heavy and light nuclei is currently a topic of high interest. The interest is stimulated mainly by the possibility of extracting the value of the nuclear matter incompressibility coefficient (which is important for studies of the nuclear equation of state, neutron stars, supernova explosions, and heavy ion reactions [2]) from knowledge of ISGMR strength distributions and centroid energies in nuclei throughout the periodic table [3–6]. The isoscalar giant quadrupole resonance often needs to be studied simultaneously with the ISGMR due to the strong overlapping of their transition strengths.

The main experimental tool for studying isoscalar giant resonances in general and the ISGMR, in particular, is inelastic α-particle scattering. There are several reasons for this. First, α particles are selective as to exciting isoscalar modes which either eliminates or greatly reduces the interference of other excitations. Second, angular distributions of inelastically scattered α particles at small angles are characteristic for some of the multipolar modes which makes it possible to identify contributions from these excited modes in the experimentally measured angular distributions.

As a result of extensive experimental studies, significant amounts of the ISGQR and ISGMR strength was observed below 40 MeV excitation energy in all studied $A>90$ nuclei [7–9] and resonance energies as functions of nuclear mass number were found to be 60–65 $A^{-1/3}$ MeV for the ISGQR and $\sim$80 $A^{-1/3}$ MeV for the ISGMR. However, until recently, not more than 30% of the ISGMR strength was found in practically all $A<90$ nuclei [9]. This, to a great extent, could be attributed to the fragmentation of ISGMR strength in light nuclei so that large parts of the ISGMR energy-weighted sum rule are imbedded into the very poorly known continuum and subtracted as a result of the experimental procedure.

Recently, experimental studies of isoscalar giant resonance excitations in nuclei ranging from ^{12}C to ^{208}Pb were performed at Texas A&M University using 240 MeV bombarding energy α particles [10–13]. Excellent peak-to-continuum ratios in the observed inelastic scattering spectra were obtained and the ambiguity associated with the continuum subtraction was notably reduced. New conclusions regarding isoscalar monopole strength distributions in some $A<90$ nuclei have been drawn [11,12]. In particular, it has been reported [11] that almost 100% of the ISGMR energy-weighted sum rule was exhausted in ^{40}Ca below 30 MeV excitation energy which almost triples previous experimental results [14,15]. At the same time, in ^{58}Ni, only about 30% of the ISGMR strength was located for $E_x<30$ MeV [10].

The problem of missing monopole strength in ^{58}Ni was addressed by Satchler and Khoa [16], who examined the theoretical aspects of the analysis of inelastic α-particle scattering data. Based upon the most realistic folding models, the authors came to the conclusion that up to 50% of the ISGMR sum rule limit has been observed in ^{58}Ni. However, these folding model calculations were done assuming that the collective model form is an adequate approximation for the transition densities.

In this work we consider the excitation of the ISGMR and ISGQR in several nuclei by inelastic scattering of 240 MeV α particles and carry out a realistic microscopic analysis of the reaction cross sections based on recent and highly accurate experimental data. On the one hand, it is interesting to compare the new experimental data with the theoretical predictions based on self-consistent Hartree-Fock– (HF-) random-phase-approximation (RPA) calculations with zero-range Skyrme-type interactions. On the other hand, it is important to investigate the consequences of some assumptions made in the experimental analysis itself, in particular, the assumption of collective model radial shapes of transition

densities. This assumption needs to be carefully examined, especially for light nuclei since, as was reported in [17], it may lead to an overestimation of the isoscalar monopole (E0T0) energy-weighted sum rule (EWSR) by up to 30%.

The purpose of this paper is twofold. First, we give a full microscopic description of isoscalar monopole excitations in ^{28}Si, ^{40}Ca, ^{58}Ni, and ^{116}Sn based on self-consistent HF-RPA calculations. We use the SL1 parametrization of the Skyrme interaction [18] which gives a value of the nuclear matter incompressibility of 230 MeV. The SL1 interaction, which is associated with an effective mass of 0.55, was fitted to the available experimental data on the E0T0. However, the theoretical results for the E2T0 obtained with this interaction [19] are somewhat higher than the corresponding experimental data by 3–5 MeV. Second, we give a theoretical description of 240 MeV α-particle scattering reactions within the folding model distorted-wave Born approximation (DWBA) and compare our HF-RPA results with the conclusions drawn from the experimental-like analysis of cross sections. We investigate how the approximate forms of the isoscalar monopole (E0T0) and isoscalar quadrupole (E2T0) transition densities deduced from the collective model may affect the results regarding the strengths and excitation energies of E0T0 and E2T0 resonances.

II. HARTREE-FOCK–RANDOM-PHASE-APPROXIMATION FORMALISM

The delta-functional coordinate dependence of the Skyrme interaction makes it possible to give a simplified coordinate space formulation of the RPA in terms of Green's functions [20]. The RPA Green's function $G^{RPA}(\mathbf{r},\mathbf{r}',E)$ is found from the equation

$$G^{RPA}(\mathbf{r},\mathbf{r}',E)=G^0(\mathbf{r},\mathbf{r}',E)+\int d\mathbf{r}_1 d\mathbf{r}_2 G^0(\mathbf{r},\mathbf{r}_1,E)V_{ph}(\mathbf{r}_1,\mathbf{r}_2)\times G^{RPA}(\mathbf{r}_2,\mathbf{r}',E), \quad (1)$$

where $G^0(\mathbf{r},\mathbf{r}',E)$ is the Green's function of the free system and $V_{ph}(\mathbf{r}_1,\mathbf{r}_2)$ is the zero-range particle-hole interaction.

In order to be able to consider both closed-shell and open-shell nuclei, we follow the ansatz proposed in Ref. [21] and evaluate the free-system Green's function from

$$G^0(\mathbf{r},\mathbf{r}',E)=\sum_{p,h}\theta_h(1-\theta_p)\times\left[\frac{\phi_p(\mathbf{r})\phi_h^*(\mathbf{r})\phi_p^*(\mathbf{r}')\phi_h(\mathbf{r}')}{E-\varepsilon_p+\varepsilon_h+i\Gamma/2}-\frac{\phi_h(\mathbf{r})\phi_p^*(\mathbf{r})\phi_h^*(\mathbf{r}')\phi_p(\mathbf{r}')}{E+\varepsilon_p-\varepsilon_h+i\Gamma/2}\right], \quad (2)$$

where $\phi_k(\mathbf{r})$ and ε_k are the Hartree-Fock single-particle wave functions and energies, $\Gamma/2$ is the smearing half-width (taken to be 1.0 MeV), θ_h and θ_p are the occupation numbers of the Hartree-Fock single-particle states, and the summation over p and h states is extended to the entire single-particle spectrum. In our calculations we include single-particle states up to an excitation energy of 100 MeV (discretized continuum). For a spherically symmetric nucleus, the occupation numbers can be taken simply as $\theta_\lambda=N_\lambda/(2j_\lambda+1)$, where N_λ and j_λ are the number of nucleons on the single-particle orbital λ and their angular momentum, respectively. The expression for $V_{ph}(\mathbf{r}_1,\mathbf{r}_2)$ in terms of Skyrme-force parameters can be found elsewhere [20,22,19].

The quantities characterizing nuclear excitations can easily be found using the RPA Green's function (1). In particular, the transition strength distribution $S(E)$ and its energy moments M_k for the one-body excitation operator $Q=\sum_{i=1}^{A}f(\mathbf{r}_i)$ are obtained from

$$S(E)=-\frac{1}{\pi}\int d\mathbf{r}\,d\mathbf{r}'\,f^*(\mathbf{r})\mathrm{Im}[G^{RPA}(\mathbf{r},\mathbf{r}',E)]\,f(\mathbf{r}'), \quad (3)$$

$$M_k=\int_0^\infty dE\,E^k S(E)=-\frac{1}{\pi}\int dE\,E^k\times\left[\int d\mathbf{r}\,d\mathbf{r}'\,f^*(\mathbf{r})\mathrm{Im}[G^{RPA}(\mathbf{r},\mathbf{r}',E)]\,f(\mathbf{r}')\right], \quad (4)$$

while the transition density $\delta\rho(\mathbf{r},E_\nu)$ for the excited state $|\nu\rangle$ having the excitation energy E_ν and the half-width $\Gamma/2$ is given by

$$\delta\rho(\mathbf{r},E_\nu)=\pm\left[-\frac{\Gamma}{2}\mathrm{Im}[G^{RPA}(\mathbf{r},\mathbf{r},E_\nu)]\right]^{1/2}. \quad (5)$$

III. "MICROSCOPIC" VS "MACROSCOPIC" DESCRIPTION OF α SCATTERING WITHIN THE FOLDING MODEL DWBA

The distorted-wave Born approximation has been widely used in experimental studies in order to give a theoretical description of low-energy scattering reactions and, thus, analyze measured cross sections of scattered probes. The folding model approach [23,24] to the evaluation of optical potentials appears to be quite successful and is extensively used at present in theoretical descriptions of α-particle scattering [16,25–27]. This approach provides a direct link to the description of α-particle scattering reactions based on microscopic HF-RPA results.

Within the folding model approach, the optical potential $U(r)$ is given by

$$U(r)=\int d\mathbf{r}'V(|\mathbf{r}-\mathbf{r}'|,\rho_0(r'))\rho_0(r'), \quad (6)$$

where $V(|\mathbf{r}-\mathbf{r}'|,\rho_0(r'))$ is the nucleon-α interaction, which is generally complex and density dependent, and $\rho_0(r')$ is the ground-state (Hartree-Fock) density of a spherical target nucleus. It is customary to adopt a certain form for the

nucleon-α interaction and obtain the interaction parameters from the fit to experimentally measured elastic angular distributions. In this work, both real and imaginary parts of the nucleon-α interaction are chosen to have the Gaussian shape with density dependence:

$$V(|\mathbf{r}-\mathbf{r}'|,\rho_0(r'))=-V(1+\beta_V\rho_0^{2/3}(r'))e^{-|\mathbf{r}-\mathbf{r}'|^2/\alpha_V} - iW(1+\beta_W\rho_0^{2/3}(r'))e^{-|\mathbf{r}-\mathbf{r}'|^2/\alpha_W}. \tag{7}$$

The parameters V, β_V, α_V and W, β_W, α_W in Eq. (7) are determined by a fit of the elastic scattering data. A similar form of the nucleon-α interaction was used in Ref. [16] where scattering of 129 and 240 MeV α particles by ^{58}Ni was considered.

For a state with multipolarity L and excitation energy E, the radial form $\delta U_L(r,E)$ of the transition potential can be found from

$$\delta U(r,E)=\int d\mathbf{r}'\,\delta\rho_L(\mathbf{r}',E)\left[V(|\mathbf{r}-\mathbf{r}'|,\rho_0(r')) + \rho_0(r')\frac{\partial V(|\mathbf{r}-\mathbf{r}'|,\rho_0(r'))}{\partial\rho_0(r')}\right], \tag{8}$$

where $\delta\rho_L(\mathbf{r}',E)$ is the transition density for the considered state.

At this point, we can distinguish between the microscopic and the macroscopic approaches to the α-particle scattering description based on the folding model. Within the ''microscopic'' approach, both the ground-state density and the transition density which enter Eqs. (6) and (8) are obtained from the self-consistent Hartree-Fock–RPA calculations. Within the ''macroscopic'' approach, the transition densities are assumed to have energy-independent radial shapes and are obtained from the ground-state density using the collective model. In particular, the so-called Tassie and Bohr-Mottelson radial shapes of the transition densities [28] are used in experimental studies of ISGMR ($L=0$) and ISGQR ($L=2$) excitations:

$$\delta\rho_{L=0}(r)=-\alpha(E)\left(3\rho_0(r)+r\frac{d\rho_0(r)}{dr}\right), \tag{9}$$

$$\delta\rho_{L=2}(r)=-\delta_{L=2}(E)\frac{d\rho_0(r)}{dr}, \tag{10}$$

where the energy-dependent factors $\alpha(E)$ and $\delta_{L=2}(E)$ are determined by fitting measured inelastic cross sections. The amounts of E0T0 or E2T0 strengths concentrated in a given resonance state can then be deduced from knowledge of $\alpha(E)$ and $\delta_{L=2}(E)$ in a straightforward manner, bearing in mind that for the state E_R that exhausts 100% of E0T0 or E2T0 EWSR the corresponding coefficient is given by [28]

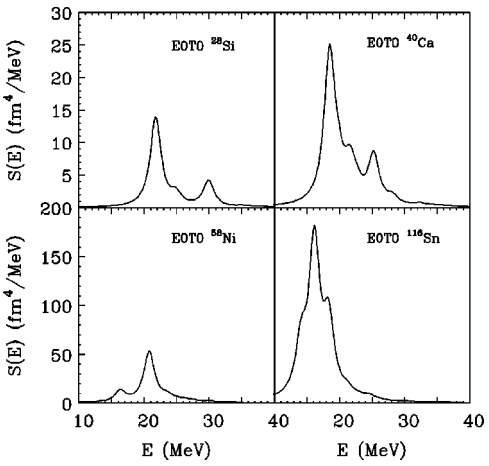

FIG. 1. Isoscalar monopole strength distributions in ^{28}Si, ^{40}Ca, ^{58}Ni, and ^{116}Sn obtained from the self-consistent HF-RPA calculations.

$$\alpha^2(E_R)=2\pi\frac{\hbar^2}{mA\langle r^2\rangle E_R}, \tag{11}$$

$$\delta^2_{L=2}(E_R)=\frac{25}{8}\frac{2\pi\hbar^2}{mAE_R}\frac{\langle r^2\rangle}{\langle r\rangle^2}, \tag{12}$$

with m, A, and $\langle r^K\rangle$ being the nucleon mass, the number of nucleons in the excited nucleus, and the Kth moment of the ground-state density, respectively.

It is not clear that the collective model results (9) and (10) are good approximations for the E0T0 and E2T0 transition densities, especially in lighter nuclei. In the following, we test these approximations by performing a folding-model–DWBA analysis of α-particle scattering by several nuclei ranging from ^{28}Si to ^{116}Sn.

IV. RESULTS AND DISCUSSION

The numerical solution of Eq. (1) using Eq. (2) and the SL1 parametrization of the Skyrme interaction [18] is the core of our microscopic calculations. A detailed description of analogous calculations can be found in the literature (see, for example, Refs. [20,22,19]). We obtain the E0T0 strength distributions from Eq. (3) using

$$Q_{00}=\frac{1}{\sqrt{4\pi}}\sum_{i=1}^{A}r_i^2$$

and

$$Q_{2M}=\frac{Z}{A}e\sum_{i=1}^{A}r_i^2Y_{2M}(\hat{\mathbf{r}}_i),$$

which are the generally accepted forms for the E0T0 and E2T0 excitation operators.

Our HF-RPA results for the E0T0 and E2T0 transition strength distributions in ^{28}Si, ^{40}Ca, ^{58}Ni, and ^{116}Sn nuclei are shown in Figs. 1 and 2. Transition strengths for the E2T0

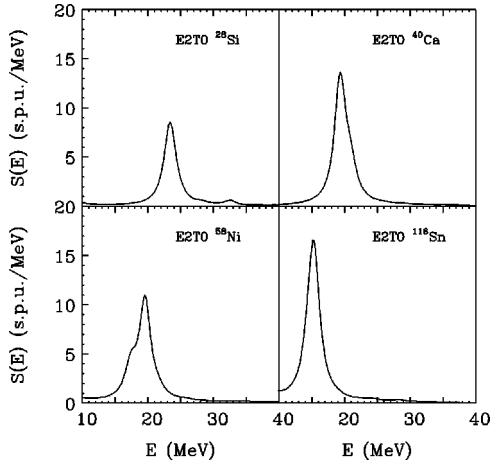

FIG. 2. Same as Fig. 1 for isoscalar quadrupole strength distributions.

excitations (Fig. 2) are given in single particle units (s.p.u.) per MeV, with

$$1\text{s.p.u.}=\frac{e^2}{4\pi}(1.2A^{1/3})^{2L}\left(\frac{3}{L+3}\right)^2, \quad L>0.$$

The resonance energies and percentages of the total E0T0 and E2T0 EWSR exhausted below 40 MeV excitation energy are given in Table I and II and compared with experimental data. A significant difference between the theoretical and experimental amounts of E0T0 EWSR exists in ^{58}Ni. Our microscopic results indicate that in ^{58}Ni, as well as in other considered nuclei, nearly 100% of E0T0 EWSR is present below 40 MeV excitation energy in contrast with no more than 50% reported in recent studies [10,16] of ^{58}Ni based on the cross section analysis.

At the next stage of our calculations, using Eqs. (6), (7) and the Hartree-Fock ground-state density, we construct the optical potential and determine the parameters of the nucleon-α interaction ($V_{\alpha n}$) of Eq. (7) by fitting experimentally measured elastic scattering angular distributions. Numerical DWBA calculations were performed with the computer program PTOLEMY [29]. Quite satisfactory fits (shown in Fig. 3) were obtained with the parametrizations of $V_{\alpha n}$ given in Table III.

TABLE I. Resonance, centroid energies, and percentages of the EWSR exhausted within the energy region $10<E<40$ MeV for ISGMR excitation in ^{28}Si, ^{40}Ca, ^{58}Ni, and ^{116}Sn nuclei. Comparison with experimental data is provided.

	^{28}Si	^{40}Ca	^{58}Ni	^{116}Sn
E_R (MeV)	21.8, 30.0	18.6, 25.2	16.4, 20.8	16.2
$\frac{M_1}{M_0}$ (MeV)	24.0	21.1	21.2	17.2
Expt.	21.5[a]	18.9[b]		
$\sqrt{\frac{M_1}{M_{-1}}}$ (MeV)	23.6	20.7	20.8	16.9
Expt.	20.7[a]	17.3[b]		
$\sqrt{\frac{M_3}{M_1}}$ (MeV)	25.4	22.6	22.6	18.6
Expt.	23.7[a]	21.3[b]		
% EWSR	91	94	96	95

[a]Reference [12].
[b]Reference [11].

TABLE II. Resonance energies and percentages of the EWSR exhausted within the energy region $10<E<40$ MeV for ISGQR excitation in ^{28}Si, ^{40}Ca, ^{58}Ni, and ^{116}Sn nuclei. Comparison with experimental data is provided.

	^{28}Si	^{40}Ca	^{58}Ni	^{116}Sn
E_R (MeV)	23.4, 32.6	19.4	19.6	15.2
Expt.	19 ± 0.2 [a]	17.7 ± 0.2 [b]	16.4 ± 0.3 [c]	13.2 ± 0.2 [c]
% EWSR	89	93	95	97

[a]Reference [12].
[b]Reference [14].
[c]Reference [8].

Having determined the parameters of the nucleon-α interaction, we calculate the cross sections of inelastically scattered α particles for the case of E0T0 and E2T0 excitations of target nuclei using the transition potential (8) and both the RPA transition densities, found from Eq. (5), and the collective model transition densities obtained using the Hartree-Fock ground state density and Eqs. (9) and (10). These transition densities are calculated for each energy value on the 0.2 MeV grid. The radial shapes of the RPA and collective model transition densities for some of the E0T0 and E2T0 resonance states are compared in Figs. 4 and 5, respectively. It can be seen that in some cases the differences in the radial shapes are quite well pronounced which affects the calculated cross sections.

In order to see more clearly the impact of radial shape differences between the microscopic and the collective

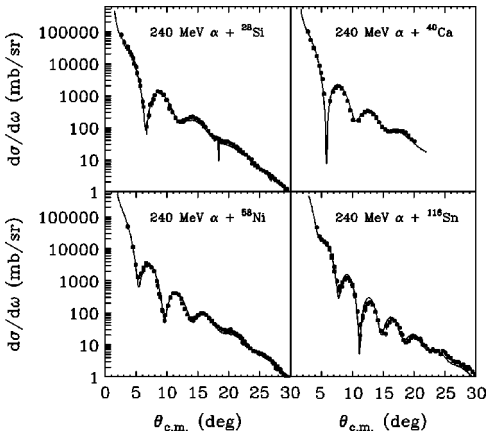

FIG. 3. Elastic angular distributions for 240 MeV α particles. Solid squares represent the experimental data taken from Refs. [10–12] and [27]. Solid lines are our fit to the experimental data using the folding model DWBA with nucleon-α interaction given in Eq. (7). The parameters of the nucleon-α interaction deduced from the fit are given in Table III.

TABLE III. Parametrizations of the nucleon-α interaction, Eq. (7), obtained by fitting experimentally measured elastic scattering angular distributions of 240 MeV bombarding energy α particles.

	V (MeV)	W (MeV)	$\beta_V=\beta_W$ (fm^2)	α_V (fm^2)	α_W (fm^2)
^{28}Si	38.0	11.2	−1.9	3.7	5.1
^{40}Ca	38.0	10.0	−1.9	3.7	5.1
^{58}Ni	38.0	11.2	−1.9	3.7	5.1
^{116}Sn	38.0	11.4	−1.9	3.7	5.1

model transition densities on the results of the cross section analysis, we assumed that the cross sections calculated using the RPA transition densities are the actual experimental data to be analyzed by performing folding-model–DWBA calculations with the collective model shapes of transition densities. In this case the extracted transition strength distributions and centroid energies can be directly compared to the corresponding results of the RPA calculations and discrepancies may occur only as a result of the approximation of transition densities by the collective model shapes.

The procedure for extracting the E0T0 strength from the cross sections is presented in Fig. 6 for ^{28}Sn. The middle panel of the figure shows 0° double differential E0T0 cross sections obtained with the RPA transition density (i.e., our ''experimental'' data). In the lower panel we show the 0° E0T0 cross sections found using the transition potential (8) with the RPA transition density (solid line) and with the collective model E0T0 transition density (9) (dashed line) normalized to 100% of the E0T0 EWSR [see Eq. (11)]. The dashed line in the upper panel of the figure is the ratio of the curve in the middle panel and the one in the lower panel. It represents the fraction of the E0T0 EWSR per unit energy reconstructed from our ''experimental'' cross sections. The solid line in the upper panel shows the actual fraction of the E0T0 EWSR per unit energy as calculated from the E0T0 transition strength distribution of Fig. 1. The reconstructed and actual E0T0 EWSRs for ^{40}Ca, ^{58}Ni, and ^{116}Sn are

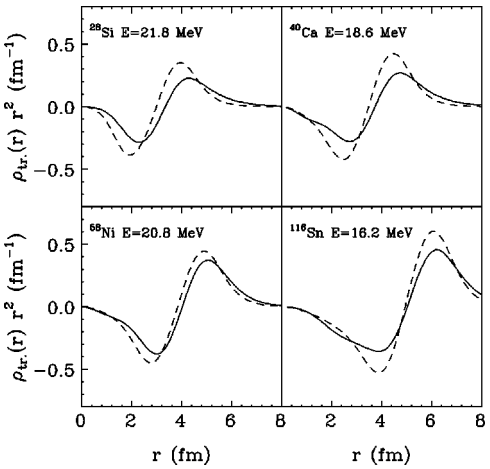

FIG. 4. Microscopic (RPA) and collective model radial shapes of transition densities for some of the ISGMR states in ^{28}Si, ^{40}Ca, ^{58}Ni, and ^{116}Sn. The solid lines are the RPA transition densities and the dashed lines are the collective model transition densities calculated from Eq. (10) using the Hartree-Fock ground-state densities. Both transition densities are normalized to a 100% of the RPA E0T0 EWSR.

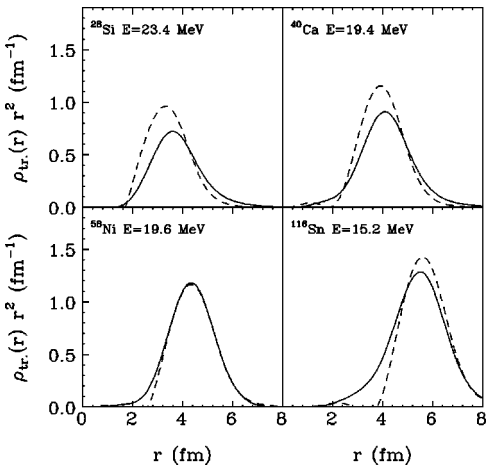

FIG. 5. Same as Fig. 4 for ISGQR states. The collective model transition densities calculated from Eq. (10) using the Hartree-Fock ground-state densities.

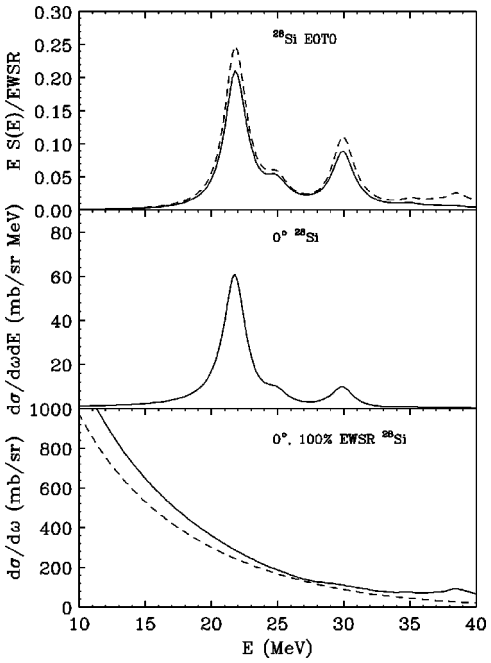

FIG. 6. Reconstruction of the E0T0 EWSR in ^{28}Si from the inelastic α-particle cross sections. The middle panel: 0° double differential E0T0 cross sections obtained with the RPA transition density (i.e., our ''experimental'' data). The lower panel: 0° E0T0 cross sections found using the collective model E0T0 transition density (dashed line) and the RPA transition density (solid line), normalized to 100% of the E0T0 EWSR. The upper panel: ratio of the curve in the middle panel and the dashed curve in the lower panel (dashed line), ratio of the curve in the middle panel and the solid curve in the lower panel (solid line). The dashed line in the upper panel represents the fraction of the E0T0 EWSR per unit energy reconstructed from our ''experimental'' cross sections while the solid line in the upper panel shows the actual fraction of the E0T0 EWSR per unit energy as calculated using the RPA.

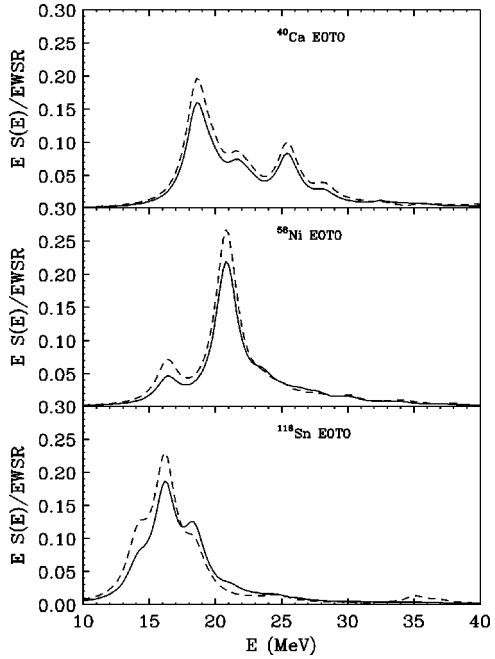

FIG. 7. Same as the upper panel of Fig. 6 for ^{40}Ca, ^{58}Ni, and ^{116}Sn.

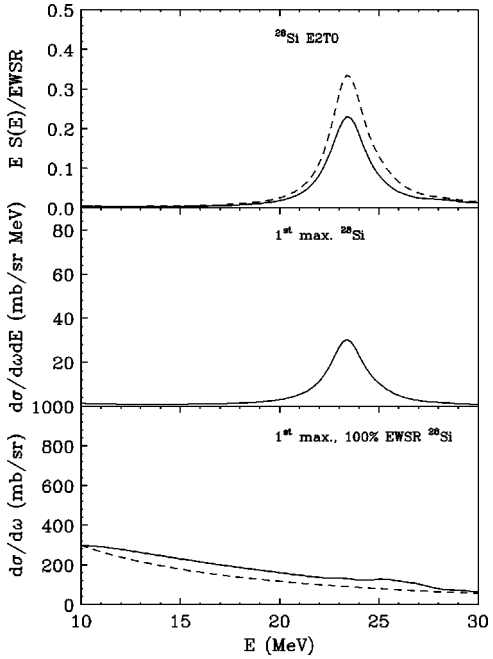

FIG. 8. Reconstruction of the E2T0 EWSR in ^{28}Si from the inelastic α-particle cross sections. The middle panel: double differential E2T0 cross sections at the first maximum obtained with the RPA transition density (i.e., our ''experimental'' data). The lower panel: E2T0 cross sections at the first maximum found using the collective model E2T0 transition density (dashed line) and the RPA transition density (solid line), normalized to 100% of the E2T0 EWSR. The upper panel: ratio of the curve in the middle panel and the dashed curve in the lower panel (dashed line), ratio of the curve in the middle panel and the solid curve in the lower panel (solid line). The dashed line in the upper panel represents the fraction of the E2T0 EWSR per unit energy reconstructed from our ''experimental'' cross sections while the solid line in the upper panel shows the actual fraction of the E2T0 EWSR per unit energy as calculated using the RPA.

shown in Fig. 7. Percentages of the E0T0 EWSR reconstructed following the above procedure are summarized in Table IV and compared to the actual percentages deduced from the HF-RPA calculations. It can be seen that the cross section analysis based on using the collective model shapes for transition densities tends to overestimate the E0T0 EWSR by up to 20%. The difference in shapes between the collective model and the microscopic transition densities can also lead to deviations of the ISGMR centroid energies deduced from the reconstructed strength distributions from the actual centroid energies obtained from microscopic calculations (see Table IV). These shifts, however, are of the order of a few percent and not very significant for the considered nuclei.

A similar procedure was applied for the case of the E2T0 excitation. In Fig. 8, taking as an example the ^{28}Sn nucleus, we show the reconstruction of the E2T0 EWSR from the E2T0 inelastic cross sections generated using the RPA transition density. The cross sections are calculated at the first maxima of E2T0 angular distributions which are located at an angle of approximately 4° and are a characteristic feature of angular distributions of inelastically α particles corresponding to the E2T0 excitation of the target nucleus. The reconstructed and actual E2T0 EWSRs for ^{40}Ca, ^{58}Ni, and ^{116}Sn are shown in Fig. 9. An interesting feature of the reconstructed E2T0 strength distributions, using the collective model transition density, is the appearance of the high-energy overtone state (see Fig. 9) which leads to an enhancement of the reconstructed E2T0 EWSR at high energies. The reason for this enhancement is the difference between the microscopic (RPA) and the collective model transition density shapes. We demonstrate this point in Fig. 10 where we compare the RPA and the collective model transition density radial shapes at the energy of the overtone state in ^{116}Sn.

As in the case of the E0T0 excitation, our results indicate that the cross section analysis of E2T0 excitation based on using the collective model transition density tends to overestimate the actual (in our case, obtained from microscopic calculations) E2T0 EWSR by up to 30%. These results for all considered nuclei are summarized in Table V. In Table V

TABLE IV. Percentages of the E0T0 EWSR exhausted by the RPA strength distribution and the ones reconstructed (REC) from 0° cross sections, following the procedure described in the text. Also shown are the centroid energies of the ISGMR (in MeV) obtained from the RPA strength distributions and the centroid energies (REC) reconstructed from 0° E0T0 cross sections.

Nucleus	Energy (MeV)	RPA (%)	REC (%)	$\frac{M_1}{M_0}$ (RPA)	$\frac{M_1}{M_0}$ (REC)	Diff. (%)
^{28}Si	10–40	91	113	24.0	24.5	2.1
^{40}Ca	10–40	94	114	21.1	21.3	0.9
^{58}Ni	10–40	96	113	21.2	20.8	1.4
^{116}Sn	10–40	95	106	17.2	16.8	2.3

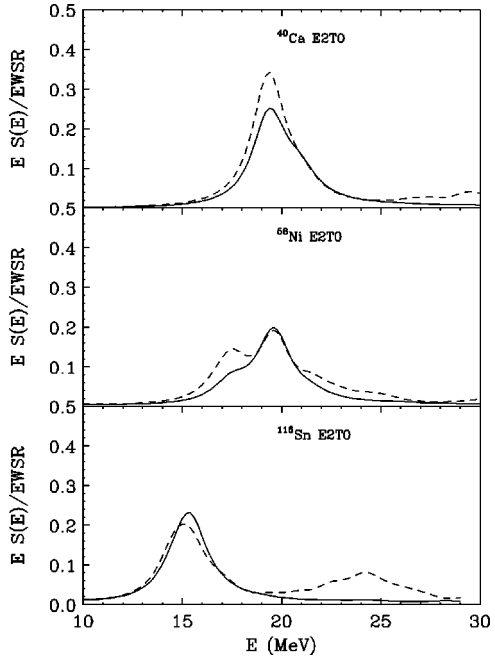

FIG. 9. Same as the upper panel of Fig. 10 for ^{40}Ca, ^{58}Ni, and ^{116}Sn.

we also show the E2T0 centroid energies obtained from the reconstructed (dashed lines in upper panel of Fig. 8 and in Fig. 9) and the actual (solid lines in upper panel of Fig. 8 and in Fig. 9) E2T0 strength distributions. As can be seen, the differences between these centroid energies do not exceed 1%.

V. CONCLUSIONS

By performing self-consistent Hartree-Fock–RPA calculations, we provided a microscopic description of isoscalar monopole and quadrupole excitations in ^{28}Si, ^{40}Ca, ^{58}Ni, and ^{116}Sn. Our results were compared with available experimental data which include the most recent measurements with 240 MeV α particles. Overall, satisfactory agreement with the experiment was obtained. However, while recent studies of the 240 MeV $\alpha+^{58}$Ni reaction were unable to locate more than 50% of the E0T0 EWSR in ^{58}Ni, our microscopic calculations showed that almost the entire E0T0 strength in this nucleus is located in the energy region $E<40$ MeV.

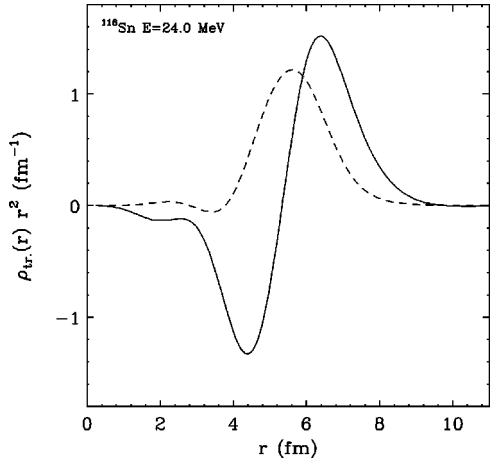

FIG. 10. Transition densities of E2T0 overtone state at $E=24.0$ MeV in ^{116}Sn. Solid line: microscopic (RPA) transition density. Dashed line: collective model transition density calculated from Eq. (10) using the Hartree-Fock ground-state density. Both transition densities are normalized to 100% of the RPA E2T0 EWSR.

TABLE V. Percentages of the E2T0 EWSR exhausted by the RPA strength distributions and the ones reconstructed (REC) from E2T0 cross sections using collective model transition density. Also shown are the centroid energies of the ISGQR (in MeV) obtained from the RPA strength distributions and the centroid energies (REC) reconstructed from the first maxima of the E2T0 angular distributions.

Nucleus	Energy (MeV)	RPA (%)	REC (%)	$\frac{M_1}{M_0}$ (RPA)	$\frac{M_1}{M_0}$ (REC)	Diff. (%)
^{28}Si	10–30	77	110	22.9	23.0	0.4
^{40}Ca	10–30	94	122	19.5	19.3	1.0
^{58}Ni	10–30	82	107	18.8	18.7	0.5
^{116}Sn	10–30	83	114	15.2	15.1	0.7

Using the density-dependent Gaussian form (7) of the nucleon-α interaction and the folding model DWBA, we gave a theoretical description of 240 MeV α-particle scattering by ^{28}Si, ^{40}Ca, ^{58}Ni, and ^{116}Sn targets. Experimentally measured elastic angular distributions were nicely reproduced by the parametrization of the nucleon-α interaction (7) given in Table III.

We tested the approximation of the E0T0 and E2T0 transition densities by the collective model shapes from Eqs. (9) and (10). Our results showed that the analysis of α-particle cross sections for the case of E0T0 and E2T0 excitations of target nuclei based on the approximations (9) and (10) tends to overestimate both the E0T0 and E2T0 EWSR in some cases by 30%. This type of cross section analysis may also shift the actual E0T0 centroid energies by up to 1% and lead to the appearance of overtone E2T0 states at high energies whose strength is enhanced compared to the actual E2T0 strength located at the same energy.

Our conclusions serve as an important guide to further experimental studies of E0T0 and E2T0 excitations. Possible overestimation of the E0T0 EWSR in the experimental analysis of cross sections due to the use of the collective model shapes for E0T0 transition densities makes the problem of missing monopole strength in ^{58}Ni even worse. Further theoretical and experimental efforts are, thus, necessary to reconcile the results of the experimental analysis with the theoretical predictions. As follows from our calculations, use of microscopic instead of the collective model radial shapes of E2T0 transition densities may be necessary for experimental studies of E2T0 excitations in order to avoid a possible enhancement of E2T0 EWSR at high energy due to the approximation (9).

ACKNOWLEDGMENTS

This work was supported in part by the U.S. Department of Energy under Grant No. FG03-93ER40773.

[1] A. Bohr and B. R. Mottelson, *Nuclear Structure* (W. A. Benjamin, London, 1975), Vol. II, Chap. 6.
[2] N. K. Glendenning, Phys. Rev. C **37**, 2733 (1988).
[3] J. P. Blaizot, D. Gogny, and B. Grammaticos, Nucl. Phys. **A265**, 315 (1976).
[4] J. P. Blaizot, Phys. Rep. **64**, 171 (1980).
[5] J. P. Blaizot, J. F. Berger, J. Decharge, and M. Girod, Nucl. Phys. **A591**, 435 (1995).
[6] J. Treiner, H. Krivine, O. Bohigas, and J. Martorell, Nucl. Phys. **A371**, 253 (1981).
[7] D. H. Youngblood, J. M. Moss, C. M. Rozsa, J. D. Bronson, A. D. Bacher, and D. R. Brown, Phys. Rev. C **13**, 994 (1976).
[8] D. H. Youngblood, P. Bogucki, J. D. Bronson, U. Garg, Y.-W. Lui, and C. M. Rozsa, Phys. Rev. C **23**, 1997 (1981).
[9] S. Shlomo and D. H. Youngblood, Phys. Rev. C **47**, 529 (1993).
[10] D. H. Youngblood, H. L. Clark, and Y.-W. Lui, Phys. Rev. Lett. **76**, 1429 (1996).
[11] D. H. Youngblood, Y.-W. Lui, and H. L. Clark, Phys. Rev. C **55**, 2811 (1997).
[12] D. H. Youngblood, H. L. Clark, and Y.-W. Lui, Phys. Rev. C **57**, 1134 (1998).
[13] D. H. Youngblood, Y.-W. Lui, and H. L. Clark, Phys. Rev. C **57**, 2748 (1998).
[14] Y.-W. Lui, J. D. Bronson, C. M. Rozsa, D. H. Youngblood, P. Bogucki, and U. Garg, Phys. Rev. C **24**, 884 (1981).
[15] S. Brandenburg, R. De Leo, A. G. Drentje, M. N. Harakeh, H. Sakai, and A. van der Woude, Phys. Lett. **130B**, 9 (1983).
[16] G. R. Satchler and D. T. Khoa, Phys. Rev. C **55**, 285 (1997).
[17] P. Chomaz, T. Suomijarvi, N. Van Giai, and J. Treiner, Phys. Lett. B **281**, 6 (1992).
[18] K.-F. Liu, H.-D. Lou, Z.-Y. Ma, and Q.-B. Shen, Nucl. Phys. **A534**, 1 (1991).
[19] K.-F. Liu, H.-D. Luo, Z.-Y. Ma, and Q.-B. Shen, Nucl. Phys. **A534**, 25 (1991).
[20] G. F. Bertsch and S. F. Tsai, Phys. Rep. **18**, 125 (1975).
[21] J. Bar Touv, A. Maolem, and S. Shlomo, Nucl. Phys. **A339**, 303 (1980).
[22] S. F. Tsai, Phys. Rev. C **17**, 1862 (1978).
[23] G. R. Satchler and W. G. Love, Phys. Rep. **55**, 183 (1979).
[24] G. R. Satchler, *Direct Nuclear Reactions* (Oxford University Press, Oxford, 1983).
[25] D. J. Horen, J. R. Beene, and G. R. Satchler, Phys. Rev. C **52**, 1554 (1995).
[26] J. R. Beene, D. J. Horen, and G. R. Satchler, Phys. Lett. B **344**, 67 (1995).
[27] H. L. Clark, Y.-W. Lui, and D. H. Youngblood, Phys. Rev. C **57**, 2887 (1998).
[28] G. R. Satchler, Nucl. Phys. **A472**, 215 (1987).
[29] M. Rhoades-Brown *et al.*, Phys. Rev. C **21**, 2417 (1980); M. H. Macfarlane and S. C. Pieper, Argonne National Laboratory Report No. ANL-76-11, Rev. 1, 1978 (unpublished).